JOURNAL OF MATERIALS SCIENCE 32 (1997) 2903–2910

Impurity-induced degradation at zirconia/sapphire interfaces

M. A. STOUGH, J. R. HELLMANN
The Pennsylvania State University, University Park, PA 16802, USA

M. S. ANGELONE
Materials Characterization Laboratory, The Pennsylvania State University, University Park, PA 16802, USA

Sapphire fibre surface damage caused by a polycrystalline zirconia coating has been analysed using scanning electron microscopy (SEM) and electron probe microanalysis (EPMA). ''Pitting'' of the sapphire surface was partially attributed to formation of a transient liquid phase (interphase) capable of local dissolution of alumina at zirconia grain contacts. Chemical etching was used to verify that the interphase material was silicate-based and resided at triple points between zirconia grains and the fibre surface. An additional crystalline calcium hexaluminate phase (hibonite) was found on some fibres. Origin of these impurities and resulting consequences of their presence are rationalized in view of observed surface modification.

1. Introduction

Ceramic fibre-reinforced ceramic matrix composites (CFCMC, or CMC for short) for structural applications have been the focus of intense research during the past decade. Relative to metal and intermetallic matrix composites, all-ceramic composites generally exhibit a number of special features. For example, most structural CMCs exhibit good mechanical properties at high temperatures ($>1000\,^{\circ}C$). In addition, reinforcing agents can exhibit high strength (sapphire fibre, $\geqslant 3$ GPa at room temperature and $\geqslant 1$ GPa at $T > 1000\,^{\circ}C$ [1]), and composites can display respectable fracture toughness (zirconia materials 5 to > 10 Mpa $m^{1/2}$ [2]) as well as strength and thermal shock resistance. Considerable work has been performed on the development of non-oxide/non-oxide composites such as SiC/Si_3N_4 [3–5], TiC/Si_3N_4 [6], and SiC/BN [7–9] systems. There also exist mixed composites (non-oxide/oxide), of which a well-known and characterized example is SiC/Al_2O_3 [10–12].

Tailoring the composite properties via the incorporation of a weak interphase such as C or BN, between the fibre and matrix, has been the focus of many studies (excellent summaries are given in references 3 and 13). However, the suitability of these CMCs for high temperature service in oxidizing atmospheres is controlled by the oxidation kinetics of these non-oxide components. When the interphase between fibre and matrix is altered by exposure to oxygen, many composite properties may be adversely affected. Therefore, efforts to study oxide/oxide composites which possess oxide interphases and overcome this atmospheric limitation have emerged.

A current prospect for oxide/oxide composites is sapphire fibre-reinforced alumina composites which exhibit minimal thermal expansion mismatch, excellent chemical compatibility and inherent oxidation resistance [12–16]. The development of sapphire fibre-reinforced alumina with ideal thermal and mechanical properties is hampered by strong interfacial bonding and fibre degradation, leading to low fracture toughness and strength, respectively. To combat this, coatings have been developed which aim to mitigate these liabilities; but, at the same time coatings generally introduce other processing concerns. For example, the coating must (i) not react with the fibre, matrix, or service atmosphere (i.e. be oxidation resistant), (ii) effectively eliminate diffusion between fibre and matrix, and (iii) provide an avenue for energy dissipation during crack propagation from loading. These requirements place heavy demands on the coating; consequently, researchers in this field have investigated polycrystalline zirconia (ZrO_2) as a likely candidate [12–18].

Zirconia has demonstrated the ability to serve as a diffusion barrier and a low-energy path for crack propagation when processed via sol–gel techniques or sputter-coating, respectively. Davis *et al.* [17, 18] showed that a porous, sputter-coated ZrO_2 coating can effectively serve as a sink for propagating matrix cracks, and hence provide a toughening mechanism. It is believed also that a ZrO_2 coating prepared such that the metastable tetragonal phase is maintained after processing may enhance toughness; this is because of the martensitic transformation of ZrO_2 to the monoclinic phase at temperatures below $\approx 1000\,^{\circ}C$ during interaction with a crack tip.

Jaskowiak *et al.* [16] demonstrated that ZrO_2 coatings limited interfacial shear strengths (ISS) in ZrO_2-coated sapphire/Al_2O_3 composites to less than

0022–2461 © *1997 Chapman & Hall*

60 MPa below 1300 °C. However, above that temperature a significant increase in ISS resulted and was attributed to coating densification and grain growth, leading possibly to mechanical interlocking between the matrix, coating, and fibre surface. Additionally, it was shown that room temperature tensile strength of coated fibres decreased after heating at 1200–1400 °C, most likely due to fibre surface modifications which had occurred. Subsequent studies [19] corroborated the role of coating grain growth and fibre surface reconstruction on interfacial shear behaviour and interfacial fatigue during cyclic loading.

Interfacial degradation and surface modification of the sapphire fibre, or "pitting", is not unprecedented in the ZrO_2/Al_2O_3 system. Both Davis *et al.* [18] and Jaskowiak [14–16] witnessed interface modification after processing and/or subsequent heat treatments in air. In addition, pitting has been witnessed in Al_2O_3 platelet reinforced tetragonal zirconia polycrystals [20]. Kerans *et al.* [21] discuss the effects of a polycrystalline material in contact with a single crystal material, and the morphological changes that can be expected. The behaviour witnessed in this study complements their review of the subject as it relates to interface stability and thermodynamics, for which we refer the reader to that work and their Fig. 4 in particular.

As a consequence of the current interest in Al_2O_3/ZrO_2 composite systems, determining the cause(s) of interfacial degradation in this system is of primary concern. In the present study, ZrO_2-coated sapphire fibres were examined to identify the mechanism(s) responsible for pitting. It is speculated that pitting may lead to measured fibre strength degradation and also increases in ISS after prolonged exposure to elevated temperatures [19].

2. Experimental procedure

We obtained several coated and heat treated fibres from M.H. Jaskowiak, National Aeronautics and Space Administration–Lewis Research Center, Cleveland, OH to study pitting; they are designated Sol #1 and Sol #2 fibres. In addition, we processed our own batch of coated fibres, designated Sol #3 fibres. The samples are described in Table I. All fibre samples were processed similarly; however, those from Sol #3 (see Table I) originated from as-received unsized Saphikon single-crystal c-axis sapphire fibres that were ultrasonicated in acetone and methanol each for 10 min. The fibres were then dip-coated at a nominal rate of 8.7 ± 0.2 cm s^{-1} in a ZrO_2 sol consisting of Tosoh 99.9% ZrO_2 powder dispersed in a zirconium *n*-propoxide solution; no stabilizing oxide was added. After drying at 110 °C in air for approximately 30 min, the fibres were isothermally introduced and suspended in a vertical high-purity alumina tube furnace and pyrolized for 3–4 h at 1000 °C to convert the hydroxides to zirconia. At this point, coated fibres would be ready for composite lay-up; however, in this study coated fibres were subjected to additional heat treatments mimicking composite processing schedules. Fibres were heat treated in air at 1400 °C for 8 and 20 h in the same high-purity alumina tube furnace. A constant flow of compressed air (≈ 5 cm^3 s^{-1}) was directed over the fibres to flush away possible contaminants and maintain an oxidative atmosphere.

Scanning electron microscopy (SEM) shows (see Fig. 1) that after 8 h at 1400 °C, the polycrystalline coating is approximately 2 μm thick and consists of grains of size 1–2 μm. Debye–Scherrer X-ray analysis was performed on a coated Sol #3 fibre to confirm that monoclinic zirconia was the room temperature phase found on our coated fibres. In addition Sol #3 itself was processed, as described above for the coated fibre, and ground to +60 mesh for powder X-ray diffraction to determine crystalline phase assemblage. Fig. 2 shows the pattern with indexing for monoclinic ZrO_2. All sols and ZrO_2 powders were chemically analysed using inductively-coupled plasma emission spectroscopy (ICP–ES) for minor and trace impurities. The results appear in Table II.

After heat treatment, small sections of fibre (0.5–1 cm) were prepared for SEM and electron probe microanalysis (EPMA) by carefully removing the zirconia coating. Under a light microscope one end of the coated fibre was held fixed while the other end of the fibre was gently flexed to spall some of the coating.

TABLE I Fibres examined and their description

Designation	Saphikon[a] spool vintage	Description of sol
Sol #1	unknown	circa 1990; Strem[b] 99.9% ZrO_2 powder
Sol #2	unknown	after Sol #1; Strem 99.9% ZrO_2 powder[c]
Sol #3	567[d] (31 Jul 92) & 656 (3 Feb 93)	Penn State 1993; Tosoh[e] TZ-0 ZrO_2 powder

[a] Saphikon, Inc., Milford, NH 03055.
[b] Strem Chemicals, Inc., Newburyport, MA 01950.
[c] Different lot number.
[d] Spool 567, like spool 656, was received unsized (no protective coating); however, spool 567 fibre supply dwindled before the completion of this study, and was continued with spool 656 fibre.
[e] Tosoh Ceramics Division, Bridgewater, NJ 01807; mean particle size ≈ 0.4 μm.

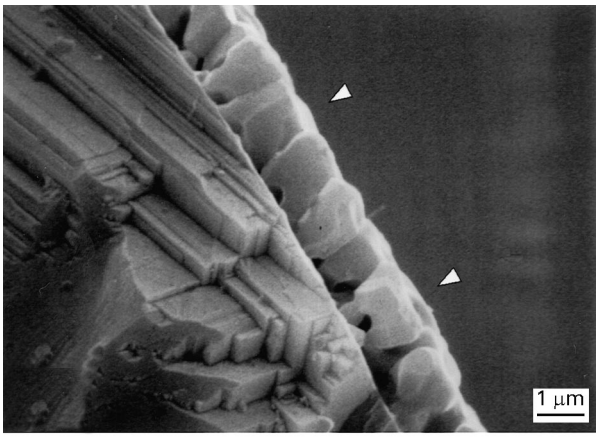

Figure 1 In this study, sol-derived polycrystalline ZrO_2 coatings (see arrows) on sapphire exhibit grains approximately 1–1.5 μm in size after heat treatment at 1400 °C for 8 h in air. The coating thickness is approximately the same size.

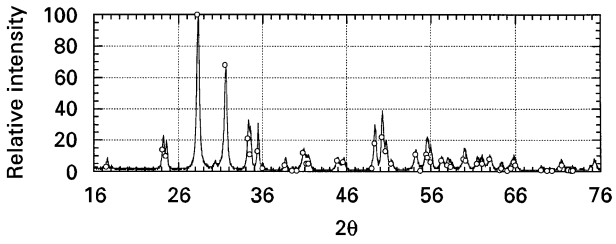

Figure 2 Powder X-ray diffraction pattern of Sol #3 solution — processed similar to a coated fibre except held at 110 °C for 6 h before pyrolysation. X-ray analysis was done to determine if impurity compounds were noticeably present. Indexed as monoclinic zirconia (JCPDS Card #37-1484, ○).

TABLE II Impurities found in ZrO_2 powders and precursor sols using ICP–ES (weight percent)

Material	Si	Ti	Na	Hf
Strem ZrO_2	0.2	0.2	< 0.02	1.8
Sol #1	0.4	0.1	< 0.02	2.0
Sol #2	0.06	0.32	0.06	1.42
Tosoh ZrO_2	< 0.02	< 0.02	< 0.05	1.85
Sol #3	0.07	0.02	< 0.05	1.61

Sapphire covered with polycrystalline zirconia appears white. When the coating is removed while under a light source, the optical transparency of sapphire provides a convenient method of judging the removal process. A sufficient area of pitted fibre surface was exposed in this manner for EPMA analyses. These fibres, herein referred to as "stripped" fibres, were mounted on a wire spindle attached to a SEM stub to provide 360° freedom of rotation about the fibre's c-axis for ample examination areas. For the EPMA analysis, only fibre samples from Table I heat treated to 1400 °C were studied since these fibres tended to exhibit the worst surface modification, as discussed later. Stripped fibres studied by EPMA were sputter-coated with carbon while those for SEM were sputter-coated with gold.

Another experiment was conducted to study the possibility of impurities entrained in the sizing material applied to sapphire fibres. Table III describes the samples studied using X-ray photoelectron spectroscopy (XPS). Ten to twelve 3-cm long fibres from each sample in Table III were scanned across the outer 2–7 nm layer of sized fibre. Sample C (unsized and uncoated fibre) was used as a reference and was the fibre source for Sol #3 coated fibres.

3. Results and discussion

3.1. Preliminary analysis

SEM was performed to qualitatively assess and visualize the degree of surface modification of sapphire fibre once-coated with polycrystalline zirconia and heat treated (i.e. a stripped sapphire fibre). Fig. 3. shows the pitted fibre surface as a function of heat treatment temperature. The pit morphology in each case (i.e. Fig. 3a, b, and c) is similar for each sol-coated fibre studied (Table I). Immediately evident is the pit size dependency on heat treatment temperature. As heat

TABLE III Description of XPS samples

Samples	Sizing	Nominal fibre diameter (μm)	Saphikon spool number	Date received
A	Early-grade methylcellulose [23]	≈ 190	56448	28 Apr 1989
B	Dow Methocel™	≈ 125	402	14 Jun 1991
C	unsized	≈ 125	567	31 Jul 1992

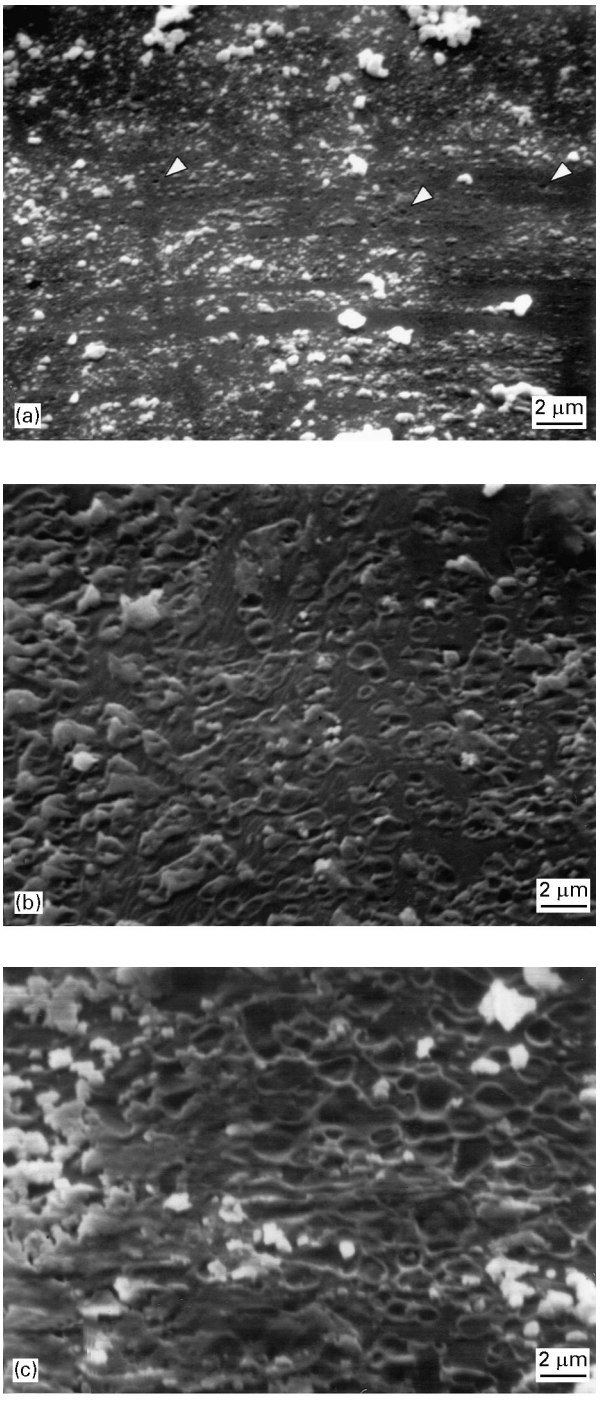

Figure 3 Sapphire fibre surface pitting after processing with a polycrystalline coating of ZrO_2. Zirconia grains are white, and the term "pit" describes the pockmarks or craters decorating the fibre surface in each micrograph. Pit size increases due to ZrO_2 grain coarsening during processing at high temperatures of (a) 1200 °C (see arrows), (b) 1300 °C and (c) 1400 °C for 8 h in air.

treatment temperature increases, pit size (referred to as the outline of each crater or "pit") also increases. Zirconia grain size increases with temperature as further densification and grain growth occur [16]. Therefore, pit size is apparently a direct function of grain growth and intimately related to the presence of ZrO_2 on the fibre surface, as demonstrated in Fig. 4. For this figure, a ZrO_2-coated sapphire fibre-reinforced alumina matrix composite processed at 1400 °C for 8 h in air was carefully sectioned such that the fibre remained attached to one side of the sample while portions of the ZrO_2 coating separated from the fibre and stayed in contact with the matrix on the opposite side. Fig. 4a and b are not mating surfaces but are representative male (ZrO_2 grains) and female (pitted fibre surface) micrographs which demonstrate the observed size dependency – each pit is approximately the same size and shape as the ZrO_2 grains.

3.2. Liquid phase evolution

Heussner and Claussen [18] speculated that pitting of alumina platelets in tetragonal zirconia polycrystalline matrices was due to impurities of Si and Mg. As Table II shows, we found Hf and Si, Ti, and Na impurities in minor and trace amounts in our sols. The possibility of Hf being a significant contributor to pitting was renounced based on complete solid solubility of HfO_2 and ZrO_2 [22]. However, the remaining elements are believed to cause liquid formation in systems involving Al_2O_3 and ZrO_2. Morgan and Koutsoutis [23] demonstrated that a liquid phase forms in the ternary system Al_2O_3–TiO_2–Na_2O at 1350 °C in the high alumina portion of the diagram (i.e., ≈ 1.0 at % Ti, ≈ 0.5 at % Na). Therefore, the elements which cause liquid formation in other alumina/zirconia systems are present as impurities in our sols. Subsequent fibre coating and pyrolysation is believed to cause segregation of these impurities to the coating/fibre interface where concentrations reach liquid-forming levels.

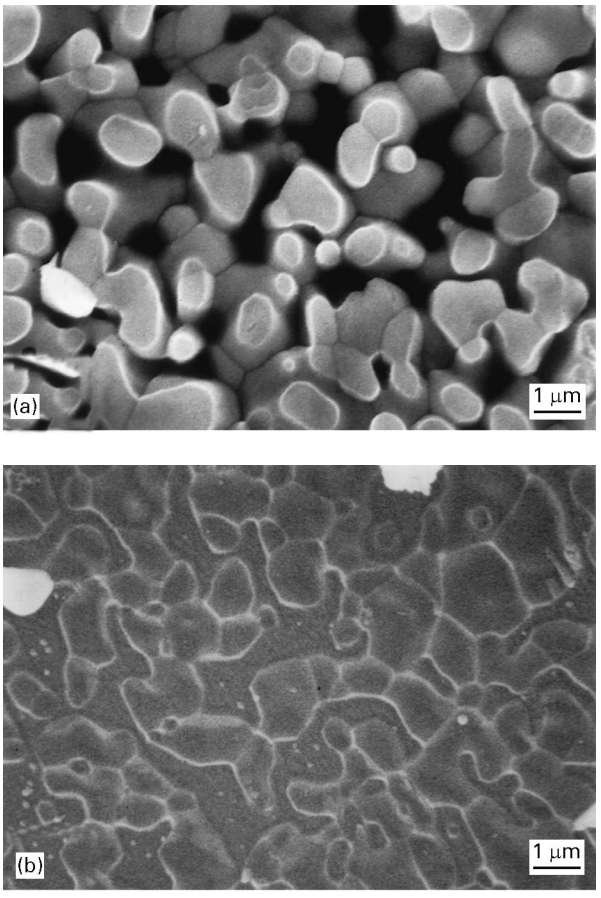

Figure 4 Representative sections of a ZrO_2-coated sapphire fibre-reinforced Al_2O_3 matrix composite showing the interface between (a) ZrO_2 grains and (b) pitted fibre surface. Note the correlation between ZrO_2 grain size and pit size as well as the relative shape of each which confirms that pitting is a direct consequence of coating/fibre contact during processing. Note: These are not matching images.

Electron probe microanalysis (EPMA) was employed as a method for determining the magnitude and distribution of segregated impurities. The experiment was conducted at two different accelerating voltages (12 and 4 keV). Electron range is directly proportional to accelerating voltage; the higher the voltage, the deeper electrons penetrate while causing characteristic X-ray emission from a host atom via electron energy transitions. Using depth distribution functions of the PAP model of Pouchou and Pichoir [24], one can calculate the maximum X-ray emission range (Re) for each element and given accelerating voltage. These values were calculated using instrument (Cameca SX-50) software (Quantiview 2.0 and Layerview) and are displayed in Table IV along with EPMA results from stripped fibres (i.e., fibres once-coated with ZrO_2 and heat treated at 1400 °C for 8 h in air). The values are reported as the range of values measured from three to six individual spot scans per sample. Each spot scan covered an area approximately two to three times larger than an average 1 μm size pit found on these stripped fibres. Due to lateral compositional variations, reporting an average value and standard deviation can be misleading; however, when necessary the arithmetic average value of data points comprising a given range was used for comparison. The data in Table IV show that Si and Na concentrations significantly increase at 4 keV accelerating voltage relative to those at 12 keV. (Ti was not detected at 4 keV since its critical excitation potential (K_α) is greater than 4 keV, and its L_α lines are weak; therefore, we presume its concentration increases proportionally with Si and Na.) This suggests that segregation of the impurities to the coating/fibre interface has occurred, causing accumulation of impurities. In other words, since the concentration of Si and Na impurities at the pitted fibre surface is equal to or greater than the corresponding concentrations in the sols (Table II), segregation and accumulation took place. In turn, the redistribution of impurities provides a source for liquid evolution at the coating/fibre interface when the system is at processing (and service) temperatures. The impurity-induced transient liquid hereafter will be termed as the interphase.

The presence and capillary behaviour of the interphase is clearly evident in the secondary electron micrograph of Fig. 5 that shows the interphase meniscus surrounding a pit. The meniscus is also seen

TABLE IV EPMA measured impurity concentrations (in p.p.m. by weight) from pitted fibre surfaces and maximum X-ray emission ranges (Re)

Impurity	Accelerating voltage (keV)	Concentration (p.p.m)			Re (μm)
		Sol #1 fibres	Sol #2 fibres	Sol #3 fibres	
Na	12	0–45[a]	0–140	DL	1.1
	4	40–350	700–1100	200–1200	0.2
Si	12	380–1210	260–380	220–310	1.1
	4	1480–7000	1350–1675	2000–5000	0.2
Ti	12	0–120	0–200	DL	0.8
	4	—[b]	—	—	—

[a] A left bound of zero indicates the concentration range reported is near the detection limit of the instrument.
[b] For Ti, 4 keV $< K_{\alpha,edge} = 4.95$ keV and L_α line emission is weak; therefore, no X-ray emission is measured. DL = below detection limit.

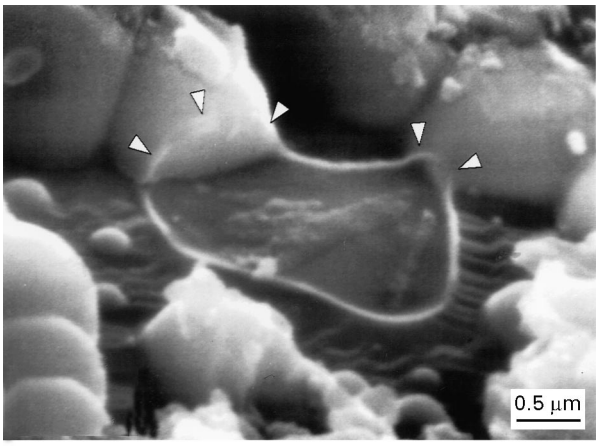

Figure 5 Liquid phase formation due to impurities (the interphase) is clearly evident. The capillary nature of the transient liquid interphase which extends around ZrO_2/ZrO_2 grain contacts (arrows) as well as ZrO_2 grain/fibre contacts can be seen. This Sol #2 fibre was heat treated (at Penn State) at 1400 °C for 20 h to further enhance the degradation which occurs.

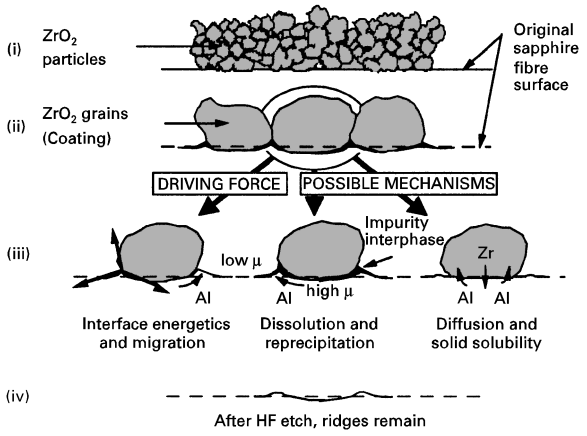

Figure 6 A schematic which suggests the evolution and morphology of fibre surface pits and the proposed effect of HF etching. The first two frames show the coating after pyrolysation (i) and after heat treatments described in the text (ii). The driving force and possible mechanisms leading to pit formation are shown in (iii), including impurity interphase evolution causing dissolution/reprecipitation phenomena (μ is chemical potential). Exposure to HF acid will effectively dissolve and remove any silicate-based interphase; hence, it is believed HF etching will alter the pit morphology in (ii) and (iii) by leaving behind the dissolved alumina surface and ridging (iv).

extending up neighbouring ZrO_2 grains (see arrows in Fig. 5). To help visualize this behaviour, Fig. 6 is presented as a suggestion of the cross-sectional view of fibre surface pit evolution. Liquid evolution at the interface results in local dissolution of the fibre surface at grain contacts, creating a pit surrounded by the interphase. (The interphase most likely contains Al from the dissolution process but distinction between matrix Al and Al in the interphase is not possible via EPMA in this experiment). During the transient liquid stage, wetting and capillarity of the interphase between individual ZrO_2 grains and the fibre surface occurs. When a ZrO_2 grain is removed, as in Fig. 5, the morphological features that remain (i.e. interphase and dissolved fibre surface) represent a fibre surface "pit".

It is commonly known that HF aggressively attacks silicate phases while remaining relatively benign to sapphire and zirconia. Therefore exposure to HF acid should alter the morphology of surface pits by removing the interphase. The proposed effect is shown in Fig. 6(iv) after the interphase has been removed by etching. Fig. 7 supports our interpretation. In an attempt to show before-and-after images, Fig. 7 is the same fibre shown in Fig. 5 but subjected to a HF etch (48% HF/51% H_2O) for one minute followed by a 15 min distilled water rinse. Exact relocation was not possible because some additional ZrO_2 grains were removed during etching and handling. It is highly conceivable that the interphase plays a critical role in securing an individual ZrO_2 grain to the fibre surface and that loss of grains could occur from the aggressive etching of the interphase by HF. Note the absence of interphase in Fig. 7 by the absence of the smooth-flowing meniscus between grain and surface regions (see arrows). Qualitatively, this suggests that the interphase was silicate-based and was attacked by the etchant. Quantitatively, EPMA analysis of an etched fibre corroborates our findings, as presented in Table V. The data were obtained as before using only the 4 keV accelerating voltage, and the comparison of percent reduction was made using the average value of the three to six data points collected for each sample.

The morphology of the etched fibre surface (Fig. 7) demonstrates that mass reconstruction occurred, as evidenced by the ridges outlining pitted regions. The

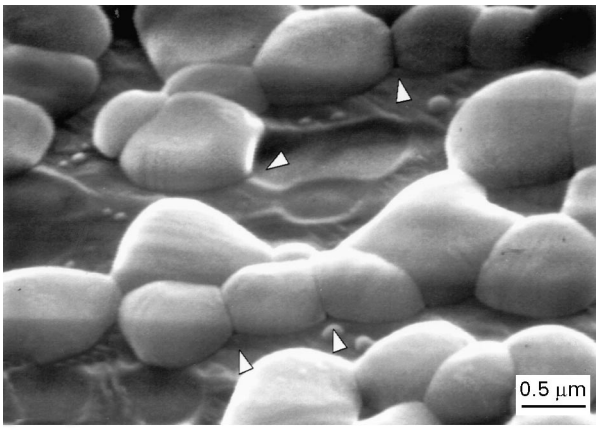

Figure 7 After subjecting the fibre in Fig. 5 to a 1 min HF acid etch followed by a 15 min distilled water rinse, evidence confirming interphase presence, composition (i.e. silicate-based), and removal can be seen here by the lack of interphase at triple points (see arrows). The smooth-flowing meniscus has been removed, revealing a sharper, more defined transition region between grain and fibre surface. Note, however, the severe degree of fibre surface modification still present.

TABLE V EPMA measured impurity concentrations (in p.p.m. by weight) of Sol #2 fibre surface before and after etching in HF

Impurity	Accelerating voltage (keV)	Concentration (p.p.m.) before etch	Sol #2 fibres after etch	Percentage reduction
Na	4	700–1100	0–240	≈ 95
Si	4	1350–1675	250–2145	≈ 36

extent of mass segregation resulting from impurity induced dissolution/reprecipitation cannot be assessed without a full understanding of the contribution made from other mechanisms, such as solid state diffusion. Other investigations are planned to examine how solid state diffusion and solubility may affect the interface between ZrO_2 and Al_2O_3.

3.3. Additional interface degradation

The vintage of fibre coated with Sol #1 and supplied to us by NASA coincides with the early studies [14, 16] of this composite system that demonstrated significant room temperature tensile strength reduction in coated fibres after processing and heat treatment. The strength loss cannot be attributed solely to pitting since younger vintage (Sol #2) fibres did not exhibit as severe strength degradation, but did display pitted surfaces [16]. During the examination of fibre pitting, an additional feature was discovered only on Sol #1 fibres. As Fig. 8 reveals, a crystalline phase had developed on the sapphire surface under the ZrO_2 coating as a function of heat treatment temperature for anneals lasting 8 h in air. The crystallite was analysed using EPMA and it was determined to have an average thickness ≈ 1.6 μm with a chemical composition given in Table VI. From the atomic concentrations the crystallite was determined to be a calcium hexaluminate (hibonite) with a charge compensated structure given approximately as $CaAl_{11.986}(Ti,Mg)_{0.014}O_{19}$. Since our initial sols did not contain

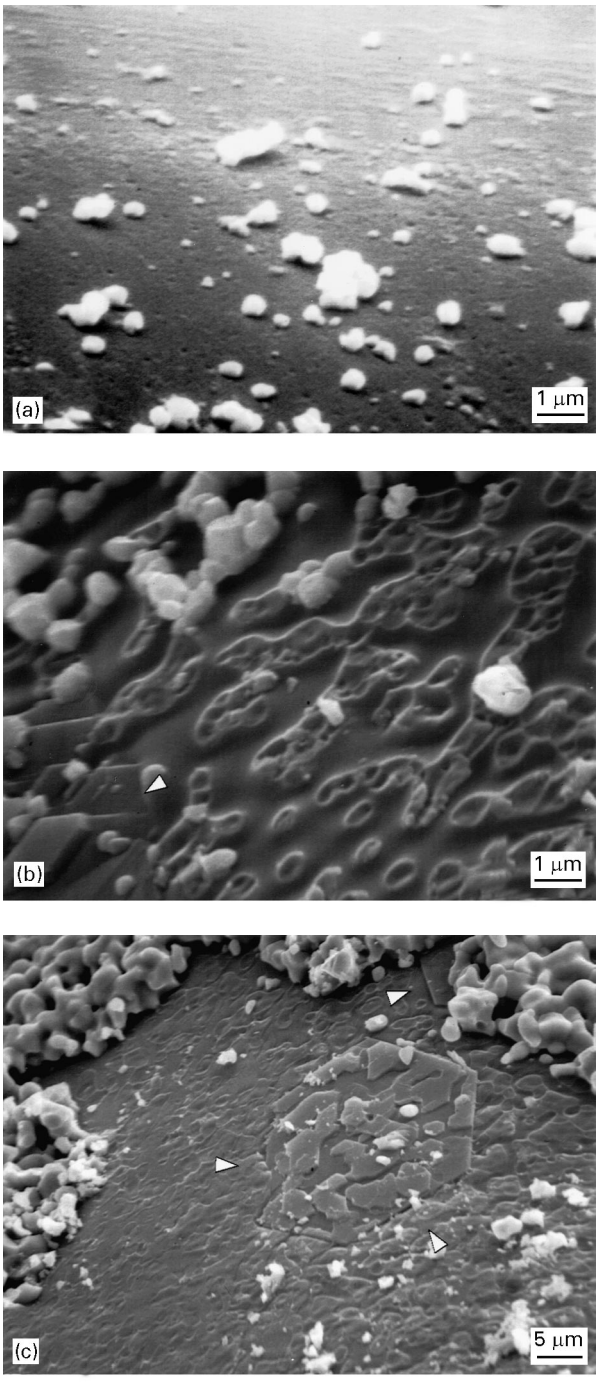

Figure 8 Development of a third phase crystallite as a function of temperature occurred on the fibre surface of Sol #1 fibres after heat treatments in air for 8 h. At 1200 °C (a), only surface pitting is evident. However, at 1300 °C (b) the recrystallization starts (arrow) and at 1400 °C (c) is fully developed on the fibre surface (arrows). Pitting also progresses. Examination of fibres like (c) indicates an areal frequency of crystallites as approximately 5% of the fibre surface.

Ca or Mg as minor impurities, we examined the methylcellulose sizing on the fibres as a potential source of impurities. Unsized and sized fibres of three different vintages were examined (Table III) which we believe coincide with the processing ages of Sol #1 and #2, and Sol #3 fibres, respectively. It is known that Sol #3 fibres were processed from the unsized fibre described in Table III. However, Sol #1 and Sol #2 fibres were supplied to us and were compared with fibres in Table III according to known processing dates. Fig. 9 is a portion of the X-ray photoelectron

spectrum for fibres listed in Table III centred on the Ca 2p peak which shows that fibres coated with the early-grade methylcellulose [25] sizing contain some residual Ca. Quite possibly, the fibres demonstrating hibonite formation may have had residual Ca present on the fibre surface after sizing removal. Of greater consequence is the discovery of hibonite crystals at fibre fracture surfaces (Fig. 10), suggesting they served as critical flaw sites and probably contributed to strength degradation in early coated fibre tensile tests [14, 15].

TABLE VI Crystalline composition (in weight percent)

Composition	Amount
Al_2O_3	88.7
CaO	8.5
MgO	1.7
TiO_2	1.1

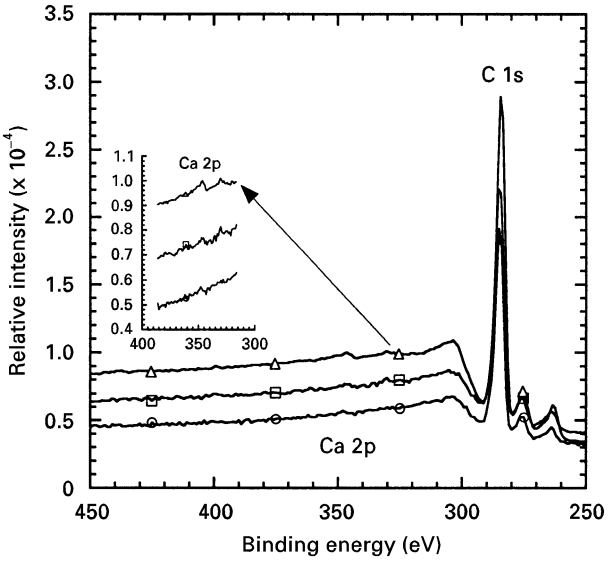

Figure 9 XPS spectra of fibres listed in Table III demonstrating the presence of Ca in the early-grade methylcellulose sizing on fibre sample A. This vintage fibre coincides with the processing age of Sol #1 fibres and therefore provides a source of Ca for hibonite formation. (○) unsized; (□) Dow Methocel™; (△) early-grade methylcellulose.

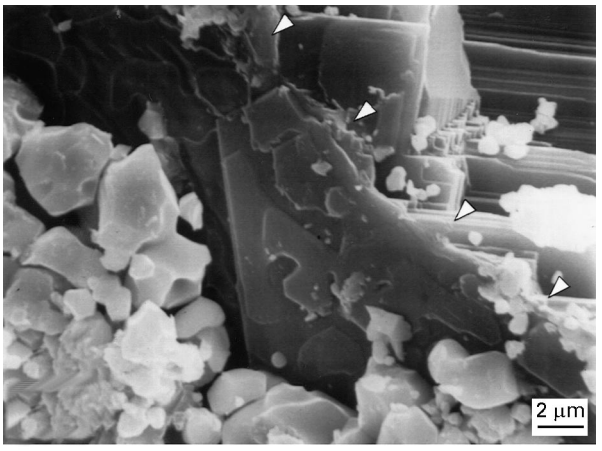

Figure 10 Hibonite crystals were found at fracture surfaces of Sol #1 fibres, suggesting that they served as critical flaw sites. The arrows delineate the edge of the fractured fibre, with the fractured surface appearing in the upper right corner of the micrograph. The remaining portion of the hibonite phase is in the centre of the micrograph.

4. Conclusions

Impurities, namely silicon, sodium and titanium were present in the zirconia sols. These impurities segregate to the coating/fibre interface in and around ZrO_2 grain contact points during composite processing at high temperatures, forming a transient aluminosilicate liquid phase. The transient liquid interphase locally dissolves Al_2O_3 (and to some extent ZrO_2) at ZrO_2 grain/fibre surface contacts and is redistributed around the contact area, contributing to pit formation. However, additional mechanisms may contribute to surface modification in this system. The formation of calcium hexaluminate (hibonite) on the fibre surface from residual impurities left behind after sizing removal in early vintage fibres has been observed to be a source of fibre degradation. Finally, the role of solid state mass redistribution and the role of mutual solid solubility on fibre surface reconstruction, in the absence of impurity-induced transient liquid phase evolution is being examined in a subsequent study.

Acknowledgements

The authors wish to express their appreciation of the support for this project from the National Aeronautics and Space Administration's HITEMP Program, Grant Number NAGW-1381. We also thank M.H. Jaskowiak, NASA-LeRC, for informative discussions and for assistance in obtaining materials.

Based in part on a thesis submitted by Matthew A. Stough for partial fulfillment of the degree Master of Science, The Pennsylvania State University, 1994. ICP–ES analysis was carried out by H. Gong, and XPS by T. Buyuklimanli, Materials Characterization Laboratory, Pennsylvania State University.

References

1. E. R. TRUMBAUER, J. R. HELLMANN, D. L. SHELLEMAN and D. A. KOSS, *J. Amer. Ceram. Soc.* **77** (1994) 2017.
2. E. H. LUTZ and M. V. SWAIN, in "Fracture mechanics of ceramics", Vol. 9 (Plenum Press, New York, 1992).
3. A. G. EVANS and D. B. MARSHALL, *Mater. Res. Soc. Symp. Proc.* **120** (1988) 213.
4. S. I. ROKHLIN, Y. C. CHU, G. V. BAAKLINI and R. T. BHATT, *Ceram. Eng. Sci. Proc.* **14** (1993) 445.
5. R. T. BHATT, *J. Amer. Ceram. Soc.* **75** (1992) 406.
6. J. J. HUANG, H. L. CHIU and M. T. LEE, *ibid.* **77** (1994) 705.
7. E. Y. SUN, S. R. NUTT and J. J. BRENNAN, *ibid.* **77** (1994) 1329.
8. L. SHEN, B. J. TAN, W. S. WILLIS, F. S. CALASSO and S. L. SUIB, *ibid.* **77** (1994) 1011.
9. S. PROUHET, G. CAMUS, C. LABRUGÈRE, A. GUETTE and E. MARTIN, *ibid.* **77** (1994) 649.
10. Y.-S. CHOU and D. J. GREEN, *ibid.* **75** (1992) 3346.
11. *Idem.*, *ibid.* **76** (1993) 1452.
12. *Idem.*, *ibid.* **76** (1993) 1985.
13. A. G. EVANS and D. B. MARSHALL, *Acta Metall.* **37** (1989) 2567.

14. M. H. JASKOWIAK, M. J. HYATT, W. H. PHILIPP, J. I. ELDGRIDGE and J. A. SETLOCK, in 3rd Annual HITEMP Review, Cleveland, October 1990, (NASA-CP 10051, 1990) p. 60.
15. M. H. JASKOWIAK, J. I. ELDRIDGE, J. B. HURST and J. A. SETLOCK, in 4th Annual HITEMP Review, Cleveland, October 1991, (NASA-CP 10082, 1991) p. 84.
16. M. H. JASKOWIAK, W. H. PHILIPP, J. I. ELDRIDGE, J. A. SETLOCK, M. E. NORKITUS and J. R. HELLMANN, in 5th Annual HITEMP Review, Cleveland, October 1992, (NASA-CP 10104, 1992) p. 59.
17. J. B. DAVIS, E. BISCHOFF and A. G. EVANS, in "Ceramic transactions", Vol. 19, edited by M. D. Sacks (The American Ceramic Society, Westerville, OH, 1991) p. 631.
18. J. B. DAVIS, J. P. A. LÖFVANDER, A. G. EVANS, E. BISCHOFF and M. L. EMILIANI, *J. Amer. Ceram. Soc.* **76** (1993) 1249.
19. J. R. HELLMANN and Y. S. CHOU, *Mater. Res. Soc. Symp. Proc.* **365** (1995) 411.
20. K. H. HEUSSNER and N. CLAUSSEN, *J. Eur. Ceram. Soc.* **5** (1989) 193.
21. R. J. KERANS, R. S. HAY, N. J. PAGANO and T. A. PARTHASARATHY, *Amer. Ceram. Soc. Bull.* **68** (1989) 429.
22. E. M. LEVIN, H. F. MCMURDIE and M. R. RESER, "Phase diagrams for ceramists" (The American Ceramic Society, Columbus, OH 1975), p. 166 Figure 4444.
23. P. E. D. MORGAN and M. S. KOUTSOUTIS, *J. Amer. Ceram. Soc.* **68** (1985) C156.
24. J. L. POUCHOU and F. M. A. PICHOIR, "Electron Probe quantitation", edited by K. F. J. Heinrich and D. E. Newbury (Plenum Press, New York, 1991).
25. J. FITZGIBBONS, Saphikon, Inc., personal communication.

Received 13 June
and accepted 23 October 1996